PCCP

Accepted Manuscript

ROYAL SOCIETY OF CHEMISTRY

www.rsc.org/pccp

Physical Chemistry Chemical Physics
CREATED USING THE RSC LaTeX PCCP ARTICLE TEMPLATE – SEE www.rsc.org/electronicfiles FOR DETAILS
ARTICLE TYPE
www. rsc.org/xxxxxx | XXXXXXXX

On the Opto-electronic Properties of Phosphine and Thiolate-protected Undecagold Nanoclusters†

Francesco Muniz-Miranda*, and Maria Cristina Menziani, and Alfonso Pedone*

Received Xth XXXXXXXXXX 20XX, Accepted Xth XXXXXXXXX 20XX

First published on the web Xth XXXXXXXXXX 200X

DOI: 10.1039/b000000x

We present here a detailed time-dependent density-functional investigation aimed at systematically dissecting the electronic spectra of two thiolate and phosphine protected undecagold nanoclusters. Calculations performed on the experimental structures of $Au_{11}(PPh_3)_7Cl_3$ and $Au_{11}(PPh_3)_7(SPyr)_3$ show that ligands give negligible contributions in the visible region. Metal→ligand charge transfer transitions appear at energies well above the visible threshold, while transitions with some small ligand→metal and ligand→ligand character occur sporadically at even higher energies. Thus, the conjugation effect between the π-electrons of the ligand and electrons of gold, recently hypothesized to interpret the spectra of phosphine and thiolate-protected nanoclusters, is not confirmed by the results of this study.

1 Introduction

Gold-based nano-particles find their use in many advanced technological applications[1], including optoelectronics[2,3], nano-medicine[4] and chemical sensors[5]. Reducing the size of gold nano-particles and approaching the nm threshold, their behavior changes from prevalently metal-like to molecule-like[6,7]. At the single-digit nanoscale, the band gap (or, more correctly, the HOMO-LUMO gap) can widen reaching values exceeding 2 eV[8]. Thus, tailoring sizes and shapes of Au-nanoparticles would allow a fine tuning of the electron conduction properties[9,10], greatly benefiting their use in opto-electronics. Due to the inherent tendency of nano-gold to aggregate (so called "aurophilicity"[11,12]), most gold nanoparticles are protected by an organic coating, usually constituted by phosphines[13], thiols[14], or both[15]. The organic ligands and their interactions with the inner metal cores play an important role in determining the three-dimensional structure of gold at the nano-scale.

† Electronic Supplementary Information (ESI) available: [TD-DFT optical spectra calculated with B3LYP, M06-HF, and B-PBE functionals on model **GIC+L**, TD-DFT spectra of PPh_3 calculated employing 6-311++G**, 6-311G, 6-31++G, 6-31G, and STO-3G basis sets are reported. A Table with 45 optical transitions is provided, as well as contour plots for 48 virtual and occupied orbitals at the cam-B3LYP/6-31++G level of theory.]. See DOI: 10.1039/b000000x/

[a] University of Modena an Reggio Emilia (UniMoRE), Dept. of Chemical and Geological Sciences (DSCG), Via Campi 183, Modena, 41125, Italy. E-mail: francesco.munizmiranda@unimore.it; alfonso.pedone@unimore.it

Furthermore, it has been very recently observed that also the electronic properties of the gold cores are affected and modulated by the organic environment that surrounds them,[16,17] particularly if the latter is composed by aromatic molecules, like, for example, triphenylphosphines and thiopyridines. Very recently Wu and Jin[16] provided clues of a conjugation between π-aromatic and gold electrons in the $Au_{11}(PPh_3)_8Br_3$ nano-cluster (NC), on the basis of peculiar NMR and UV-Vis observed signatures. Wu and Jin[16] assigned the $Au_{11}(PPh_3)_8Br_3$ observed bands to the PPh_3 molecule, and explained the red-shift of these bands as due to the aforementioned conjugation between aromatic π electrons and the metal electrons. The same authors also investigated the effect played by aromatic ligands on the fluorescence of metal nanoparticles.[17] They found that surface ligands bound through sulfur atoms can influence the fluorescence by (*i*) establishing charge-transfer transitions from the ligands to the gold core and (*ii*) directly donating delocalized electrons of rich atoms or groups of the ligands to the metal core.

Therefore, understanding the effect of the nature and strength of the interactions arising between the gold surfaces and the protecting organic molecules on the optical properties of Au-based NCs is becoming fundamental and urgent for designing luminescent metal/organic particles for promising optoelectronic and nanomedicine applications.[18].

Steady-state and time-resolved UV-Vis spectroscopies are valuable tools to investigate structure and dynamics of gold nano-particles and their organic-metal inter-phases. However, the subtle interplay of several different competing effects acting at different length and time scales makes the interpretation of such spectra quite difficult. Theoretical investigations based on accurate density functional theory (DFT) and time dependent (TD) DFT calculations[19] allow a detailed characterization of ground and excited state properties of medium to large -sized molecules, (*e.g.* Refs. 20–23) metal nano-particles (*e.g.* Refs. 24–30) and hybrid organic-inorganic structures (*e.g.* Refs. 6,31–42). Thus, it is possible to dissect the UV-Vis spectra in all their contributions and investigate, in an unbiased way, the effects due to the organic protection onto the optoelectronic features of Au-based NCs containing a few hundreds of atoms.

In this paper, a systematic study of the origin of the electronic transitions of two undecagold-based NCs (*viz.* $Au_{11}(PPh_3)_7Cl_3$ and $Au_{11}(PPh_3)_7(SPyr)_3$), whose structure has been experimentally determined, will be carried out by means of TD-DFT calculations with GGA, hybrid, and range-corrected hybrid exchange-correlation functionals. Moreover, in order to understand if and how the electronic properties and optical spectra are due to the organic ligands, as hypothesized in previous experimental investigations[16], the analysis of the contributions of different moieties of the coating will be presented.

2 Undecagold nanoclusters

To the best of our knowledge, no cluster of the type $Au_{11}(PR_3)_nX_m$ (with n,m integers, R an aromatic group and X an halogen atom or a thiol group) has *both* its X-ray resolved structure *and* electronic spectrum available in literature, except for $Au_{11}(PPh_3)_7Cl_3$[43], hereafter referred as "NC1". The X-ray resolved geometry of $Au_{11}(PPh_3)_7(SPyr)_3$ (hereafter referred as "NC2") is also available in literature[44]. These two

NCs have similar metal cores, and differ mainly for their coating. Undecagold clusters with these stoichiometries were rationalized by Provorse and Aikens[28] within the "superatom" conceptual framework[8]. Defining n^*, the delocalized electron count for a closed-shell superatom complex, as

$$n^* = (N\nu)_{\mathrm{Au}} - W - q \quad , \tag{1}$$

with N and ν the total number and the atomic valence of Au atoms, respectively, W the total number of monovalent electron-withdrawing group bound to gold atoms (Cl atoms in the case of NC1, SR groups in the case of NC2), and q the overall charge of the complex in units of $|e|$ (in these cases, zero), n^* gets a value of 8 for the NCs investigated here. A count of 8 delocalized electrons is correlated to a particular stability for approximately spherical particles, ideally resembling the closed shell of noble gases. The experimental UV-Vis spectrum[43] of $Au_{11}(PPh_3)_7Cl_3$ is very similar to the one reported by Wu and Jin[16] for $Au_{11}(PPh_3)_8Br_3$, showing two peaks at $\sim$ 316 and 406 nm and a (almost unnoticeable) shoulder between 450 and 550 nm[43], thus being a very reasonable test case to investigate computationally the extent of the assumed conjugation[16] in phosphine-protected undecagold NCs.

3 Computational Methods

All TDDFT calculations have been performed by using the `Gaussian09` package.[45] Four exchange-correlation functionals, namely the GGA B-PBE functional that combines the B88[46] exchange and the PBE[47] correlation functionals, the widely employed global hybrids B3LYP[48,49], the M06-HF[50], as well as the range-separated hybrid cam-B3LYP[51] have been employed to simulate the absorption spectrum of NC1. Instead, we employed just the cam-B3LYP functionals for NC2.

We anticipate that three functionals (*viz.* cam-B3LYP, B3LYP, M06-HF) yield similar TDDFT spectra for each model of NC1, differing essentially only for the position of the two peaks on the wavelength scale, with B3LYP providing the best positions accuracy in reproducing the wavelength of the peaks. B-PBE yields a slightly different spectrum shape. Due to the fact that cam-B3LYP usually better reproduces charge-transfer transitions[52,53], only spectra simulated with this functional (on 200 $S_0 \rightarrow S_n$ transitions) are reported here for sake of clarity. Fig.S1 of the ESI shows results obtained with B3LYP, M06-HF, and B-PBE (on 100 transitions) on NC1, along with discussion regarding the other tested functionals.

The computed spectra reported here are shifted by +50 nm, in order to better match the experimental spectra of NC1. The spectrum translation in the wavelengths domain is a widely employed procedure to ease comparison with the experiment (see for example Ref. 22,54,55). This wavelength translation results in a non-linear scaling of the energies. We notice that the scaling of frequencies (linear and non-linear) is also a widely adopted procedure in reporting computed vibrational spectra[56–59]. The wavelengths have not been shifted in Table 2, nor in the ESI.

The adopted pseudo-potential for gold atoms is an improved version[60] of the commonly used small core LanL2DZ (here referred to as "mod-LanL2DZ") with added optimized n+1 $|p\rangle$ states to the basis set, imported in the calculations through Basis Set Exchange[61]. These computational choices were previously validated by benchmarking more than 20 functionals and 5 pseudo-potentials on three gold NCs (two of them being

NC1 and NC2)[36]. The solvent in which the optical experimental spectrum of NC1 has been acquired (dichloromethane) has been simulated with a linear response polarizable continuum model[62]. Dichloromethane is also the solvent used for the cyclic voltammetry measurements on NC2. Since the number of atoms of the full NC is very large (>250) for excited-states investigations, test TD-DFT calculations have been performed in order to choose the optimal basis set for PPh_3, as reported in Fig.S2 of the ESI. The 6-31++G basis set represents the best compromise between accuracy and computational costs, and has been subsequently adopted in all the calculations reported here on simplified models for C and H atoms, while for P and Cl atoms two polarization functions have always been added (*i.e.* for them 6-31++G(d,p) has been employed). To simulate the full NCs, the smaller 6-31G basis set had to be adopted for C and H atoms to make computations feasible.

4 Results and Discussions

4.1 Models and Spectra

To dissect the electronic spectrum of NC1 into its components, five basic models (Fig.1, left panel) have been set up starting from its experimental three dimensional geometry.

1. isolated PPh_3, the organic ligand [**L**];
2. $Au_{11}(PH_3)_7Cl_3$, hereafter referred as the "Gold Inner Core" [**GIC**];
3. $Au_{11}(PH_3)_6PPh_3Cl_3$, the Gold Inner Core with one explicit ligand molecule [**GIC+L**];
4. $Au_{11}(PH_3)_6PPh_3Cl_3$ with Mulliken charges (obtained from full NC calculations with 6-31G basis set adopted for the C and H atoms) for all atoms of the other 6 missing organic ligands, with exception of the C atoms substituted by H atoms of the PH_3 groups, [**GIC+L+Q**];
5. $Au_{11}(PH_3)_5(PPh_3)_2Cl_3$, with two PPh_3 adjacent ligands [**GIC+2L**].
6. full NC

On each of these models, TD-DFT calculations have been performed to obtain the UV-Vis spectrum of NC1, as reported in Fig.2 (panels **A-E**); panel **F** of Fig.2 also shows calculations performed on the full NC1 with the reduced basis set, and in panel **G** the experimental spectra[43] are reported as reference.

The stick spectra in Fig.2 give a better view of transitions density and intensity, while their convolutions with Gaussian functions provide results more easily comparable to experimental data (blue lines).

The main bands of the isolated PPh_3 (panel **A** of Fig.2) are $\sim$ 100 nm far from those of the other models (panels **B-F**), a striking feature of these model spectra. Moreover, the shape and position of the bands (denoted with blue lines) of the models which include the gold core (panels **B-F**) are very similar among them: the *higher* energy peak (*i.e.* the peak found at *shorter* wavelengths) is somewhat slightly modified passing from the **GIC** model (panel **B**) to the **GIC+L** model (panel **C**), albeit the lower energy band seems largely unaffected. On the contrary, transitions at shorter wavelengths are rearranged in energetics and intensity by adding a ligand to the **GIC** model (**GIC+L** model, panel **C**), but adding a second ligand to obtain model **GIC+2L** (panel **E**) induces only minor changes. Also the addition of the Mulliken charges of the other ligands (model **GIC+L+Q**, panel **D**) seems to have only minor effects,

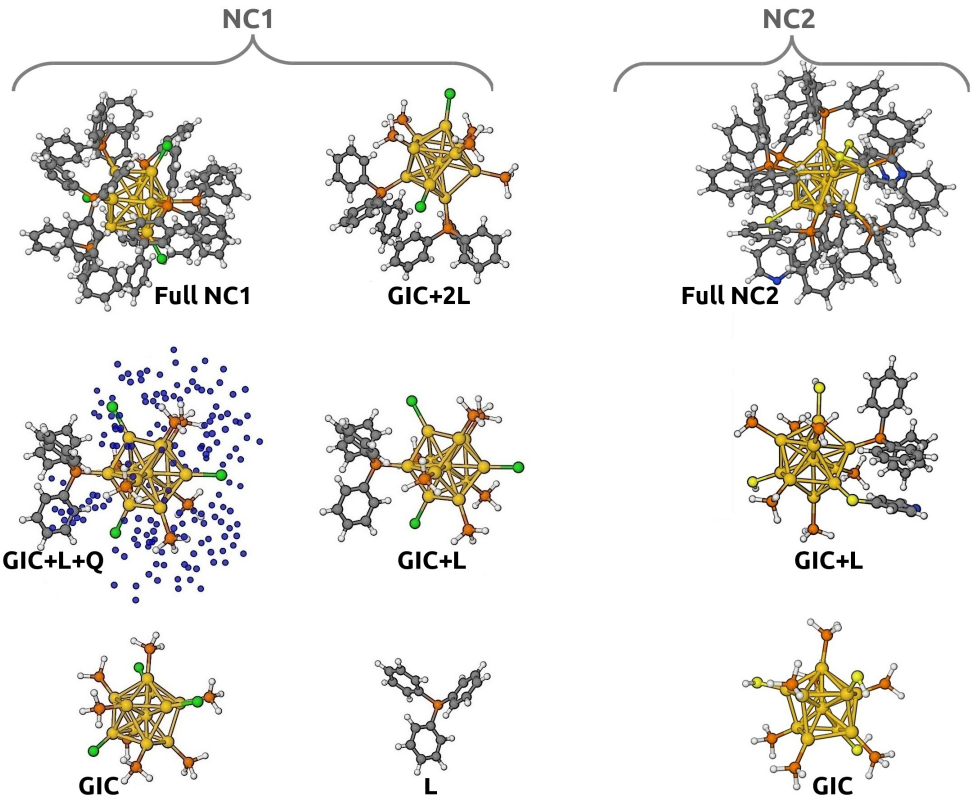

Fig. 1 The structural models adopted here to investigate NC1 (left) and NC2 (right). Acronyms are explained in the text. The picture has been generated adopting the standard CPK color scheme (H is white, C is gray, N is blue, Cl is green, P is orange, S is bright yellow, Au is dark yellow). Positions of the partial charges for NC1 (model **GIC+L+Q**, bottom left) are represented by blue dots.

both on spectra and transitions. While the 6-31++G basis set has been chosen to better reproduce the PPh_3 spectrum, calculations employing smaller 6-31G basis set for triphenylphosphine ligands (panel **F**) give rise to a spectrum whose shape and transitions are very similar to that of the **GIC+2L** model (panel **E**) and in excellent agreement with the experimental one, since it reproduces correctly the two main peaks as well as the tail at longer wavelengths. The computed spectra of the undecagold-based models (panels **B-F**) and of PPh_3 (panel **A**) yield results that can be easily compared to the experimental ones (panel **G**, magenta line and green line for NC1 and PPh_3, respectively). It appears that the electronic spectrum of this NC is mainly due to its metal core, at least in the $\lambda \geq 300$ nm range, which corresponds to the experimental range[43]. The effects induced by the organic coating seem to be of only secondary relevance.

Calculations on NC2 were limited to its corresponding **GIC**, **GIC+L**, and full NC models. In this case, L still refers to PPh_3 (whose effect is the primary interest of this paper), yet the **GIC+L** model retains a complete SPyr ligand because previous computations suggest that SPyr can establish with PPh_3 π-stacking interactions[36]. Analogous behavior is observed for NC2. In fact, even for $Au_{11}(PPh_3)_7(SPyr)_3$ the **GIC**, **GIL+L** and full NC2 models provide very similar energetics and band

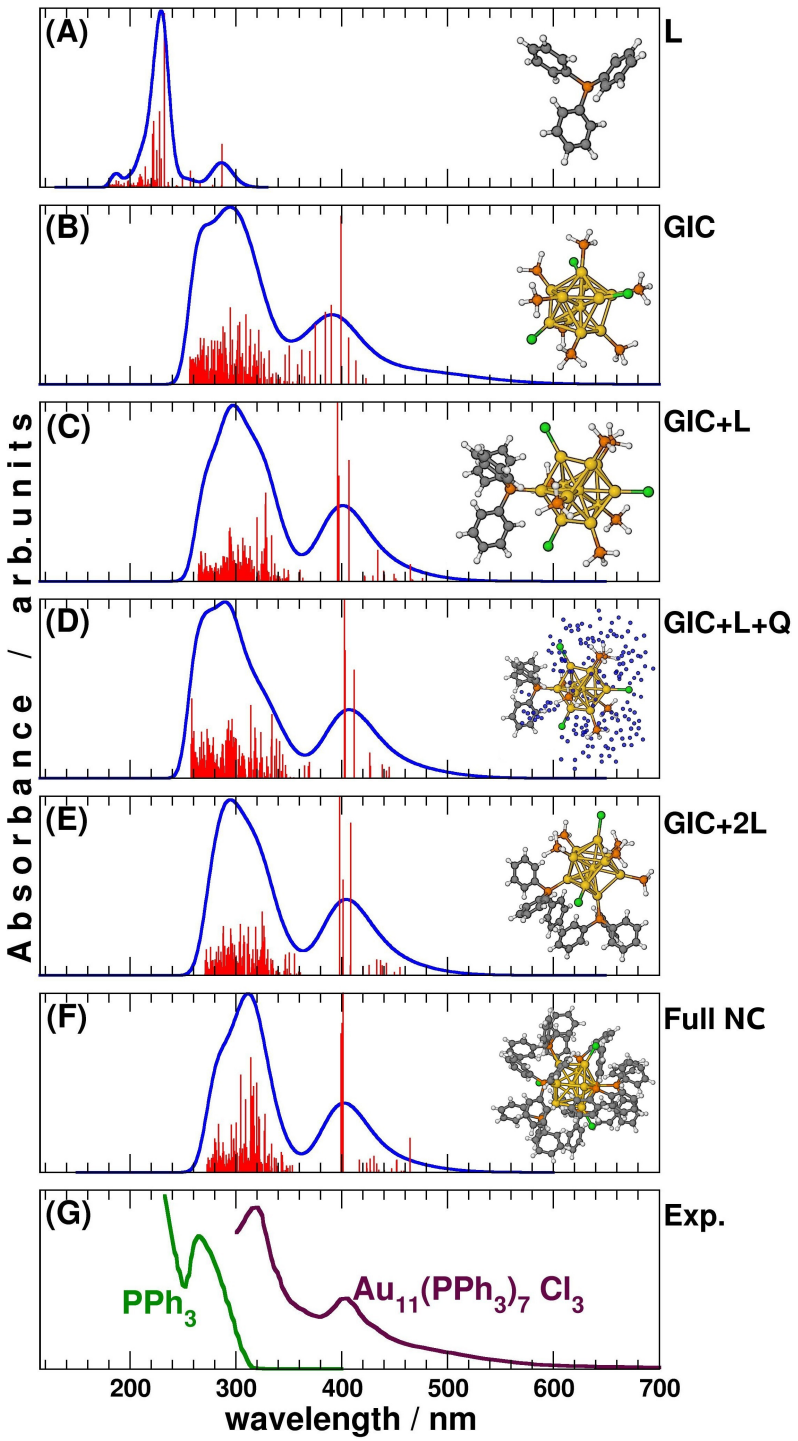

Fig. 2 **(A)** Calculated electronic spectrum on **L**, **(B)** on **GIC**, **(C)** on **GIC+L**, **(D)** on **GIC+L+Q**, **(E)** on **GIC+2L**, and **(F)** of the full NC1 (with 6-31G basis set for C and H atoms); **(G)** experimental spectrum of NC1 [Ref. 43] in toluene (magenta) and of PPh_3 [Ref. 16] in CH_2Cl_2 (green). Blue lines represent the UV-Vis spectra of the different models obtained from the convolution of 200 $S_0 \rightarrow S_n$ transitions (red sticks) with Gaussians of half-width at half-height of 0.25 eV. Wavelengths obtained for the calculated spectra (panel **A-F**) are shifted of +50 nm to super-impose them with the experimental counterparts (panels **G**); the computed values are reported in Table 2. Computations have been carried out at the cam-B3LYP/6-31++G level of theory.

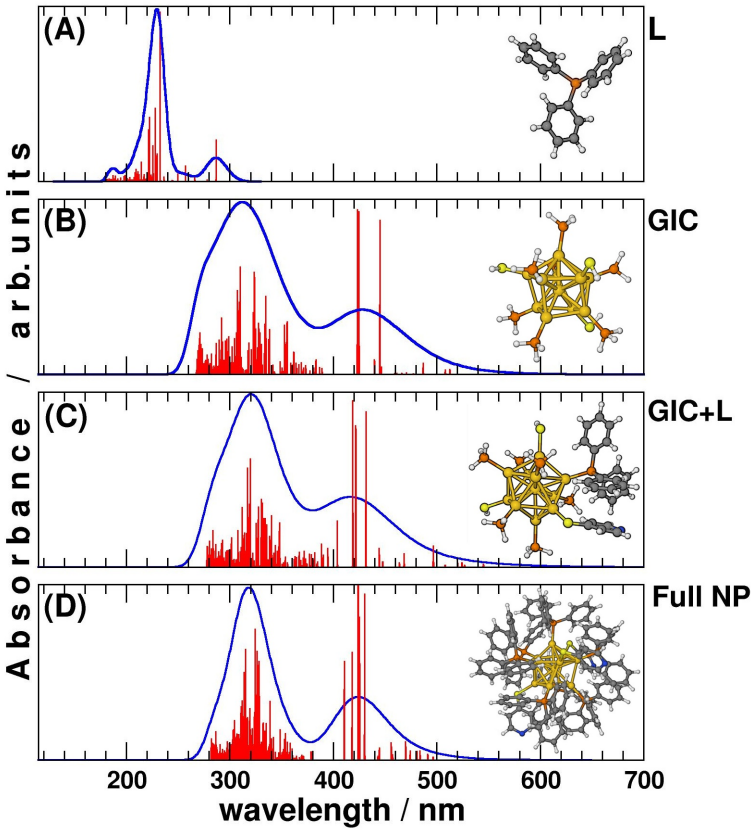

Fig. 3 **(A)** Calculated electronic spectrum on **L**, **(B)** on **GIC**, **(C)** on **GIC+L**, and **(D)** on the full NC2 (with 6-31G basis set for C and H atoms); Blue lines represent the UV-Vis spectra of the different models obtained from the convolution of 200 $S_0 \rightarrow S_n$ transitions (red sticks) with Gaussians of half-width at half-height of 0.25 eV. Wavelengths obtained for the calculated spectra (panels **A-C**) are shifted of +50 nm in analogy to Fig. 2; the computed values are reported in Table 2. Computations have been carried out at the cam-B3LYP/6-31++G level of theory.

shapes (Fig.3), despite the presence of SPyr ligands in place of Cl atoms. Figure 4 compares the absorption UV-Vis spectra of the two full NC models. The substitution of Cl ions with the thiopyridine ligands leads to redshifts of ∼20 and ∼5 nm for the main absorption bands at lower and higher energy, respectively. Concerning the optical gap (i.e. the first optical transition[63]), that of NC2 is red-shifted of about ∼60 nm (corresponding to ∼0.4 eV) with respect to NC1 and it seems to be correlated to the charge of the gold inner core. In fact, the metal core of the full NC1 is less negatively charged[36] than that of the full NC2 of more than $+0.8|e|$ (as computed from Hirshfeld charges[64], $|e|$ being the unsigned charge of the electron), probably due to the greater electronegativity of Cl atoms with respect to SR groups. This results in a more stable HOMO state for NC1 ($E^{HOMO}(NC1) - E^{HOMO}(NC2) = -0.83$ eV at cam-B3LYP level of theory). Also the LUMO of NC1 is lower in energy than the LUMO of NC2, but this effect is smaller ($E^{LUMO}(NC1) - E^{LUMO}(NC2) = -0.27$ eV at cam-B3LYP level of theory), thus resulting in an estimated net shrinking of the gap of NC2 of ∼0.56 eV, in qualitatively agreement with the energy redshift of ∼0.4 eV previously discussed. The shrinking of the optical gap is observed only for

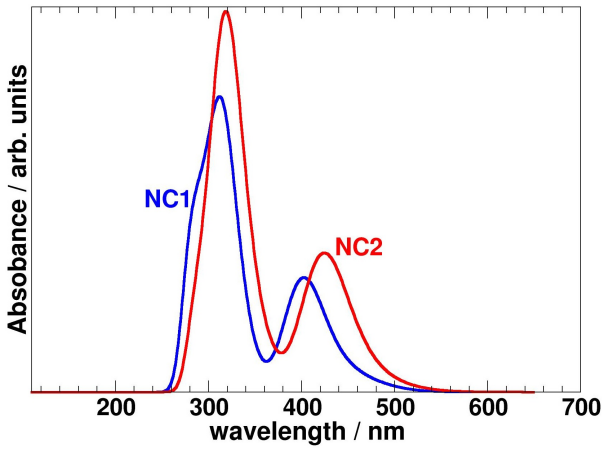

Fig. 4 Comparison between the computed spectra of full NC1 (blue line) and NC2 (red line). Each spectrum is the convolution of 200 $S_0 \rightarrow S_n$ transitions with Gaussians of half-width at half-height of 0.25 eV. Wavelengths are shifted of +50 nm in analogy to Fig. 2; the computed values are reported in Table 2. Calculations have been carried out at the cam-B3LYP/6-31++G level of theory.

Full NC models because for the simplified **GIC** models of NC1 and NC2 the computed optical gaps are indeed much closer (difference between them $\leq$0.1 eV) and the NC1 metal core is more positively charged[64] than the NC2 metal core of less than $+0.3|e|$, as reported in Table 1.

The thiol ligands also somewhat affect the electronic Density of States (DoS), resolved per atomic components with the `Multiwfn` software[65] and here summarized by following Figure 5. With this procedure, it is possible to sort out the contributions due to the core and the ligands. As can be appreciated, both the total DoS and its atomic components are largely superimposable for NC1 and NC2. The virtual orbital zone (energy ≥ 0) is very similar between them, and also the components due to Au, P, and the rest of organic ligands (C, H, and possibly N atoms for NC2). Still, some differences due to Cl and S atoms can be pointed out. Cl atoms contribute to some low energy bands in NC1 ($\leq$18 eV), which are absent in NC2, while the effect of the S atoms in NC2 seems more relevant because it occurs near the HOMO-LUMO gap (centered at 0 eV in Fig. 5). In fact, while in NC1 a small gap is present among the occupied orbitals DoS (at $\sim$-3.5 eV), this gap is absent in the NC2 DoS due to the contribution of S atoms. In particular, the small peak at $\sim$3.5 eV of the NC2 DoS is due to the $|l = 1\rangle$ orbitals of S atoms, absent in NC1, which therefore help closing the gap.

Albeit the nature of the ligands (SPyr *vs* Cl) affects the charge of the metal core, and, thus, the position of the peaks in the optical spectra, the similarity between the absorption spectra of GIC and full NC models suggest that the spectra is dominated by Metal$\rightarrow$Metal transitions.

Therefore, the conjugation between aromatic π-electrons and metal electrons, advocated by Wu and Jin[16] to explain the spectra of $Au_{11}(PPh_3)_nX_3$ clusters in terms of a shifting of electronic transitions involving ligands, is not observed in the NCs studied here. However, even if of secondary importance, some small effects due to the coating are observable in the computed spectra.

4.2 Energetics of the Transitions

The analysis of the DFT-computed molecular orbitals involved into the various optical transitions for the model **GIC+L** of both clusters has been carried out to investigate the effects of ligand$-$ligand, metal$-$ligand and ligand$-$metal transitions.

Table 2 lists the features of the 8 more significant $S_0 \rightarrow S_n$ transitions (of the 200 investigated in this work) of the **GIC+L** model of NC1 (higher panel). The Kohn-Sham molecular orbitals interacting in these transitions are represented as con-

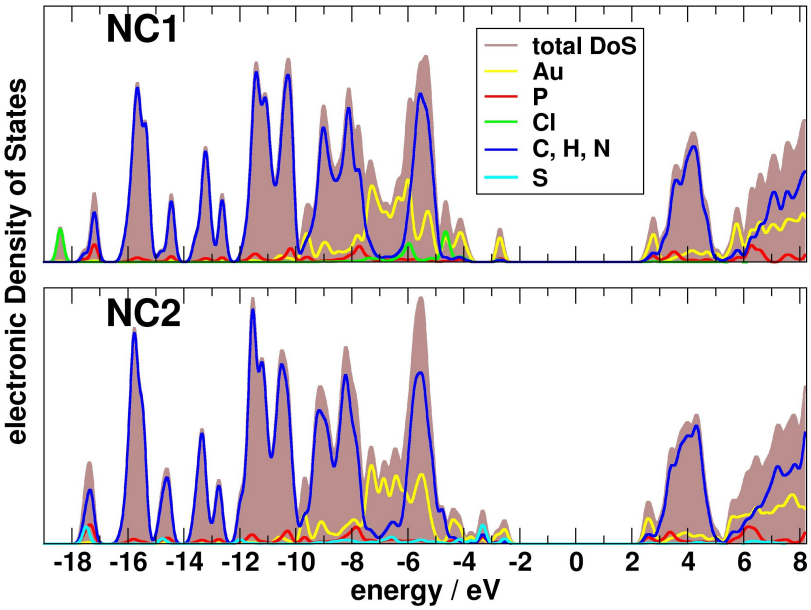

Fig. 5 Total and partial Density of electronic States for the full NCs. The center of the band gap has been set to 0 eV for clarity porpuses. Calculations were performed at the cam-B3LYP/6-31++G level of theory.

	GIC model		Full NCs	
	NC1	NC2	NC1	NC2
Au_{11}	-1.048	-1.319	-1.276	-2.079
P	+0.327	+0.302	+0.352	+0.294
S	—	-0.264	—	-0.236
Cl	-0.414	—	-0.401	—

Table 1 Partial average Hirshfeld charges of some selected elements for **GIC** and full NC models of NC1 and NC2 in unsigned electron charge (*i.e.* $|e|$). The charge of Au_{11} is the sum of all metal charges. Computations have been carried out at the cam-B3LYP/6-31++G level of theory

tour plots in Fig.6. As can be observed, at low energies ($\leq$4.5 eV, corresponding to the longer wavelength band of Fig.2) the transitions involve only orbitals localized on the metal core, with some contributions of P and Cl atoms. No significant contribution due to the aromatic molecules is apparent and only **GIC**$\rightarrow$**GIC** transitions are found. Only at energies $\geq$4.80 eV (corresponding to the shorter wavelength band of Fig.2) **GIC**$\rightarrow$**L** charge transfer bands start appearing, as in case of the transition $\boldsymbol{n}$=68, which is also one of the most intense in this range of observed energies. Some small contributions from **L**$\rightarrow$**L** and **L**$\rightarrow$**GIC** excitations occur for transitions $\boldsymbol{n}$=144 (5.44 eV) and $\boldsymbol{n}$=170 (5.60 eV), respectively. In particular, a small contribution (CI coefficient =0.10) to the 144^{th} excited state is given by the transition between the orbitals HOMO-25 (orbital #228) and LUMO+8 (orbital #262), both localized on the ligand molecule. This transition is blue-

NC1

n	**⟨occ.orb.|**	→	**|virt.orb.⟩**	**CI coeff.**	**osc.str. ($\cdot 10^{+4}$)**	**energy/eV**	**λ/nm**
1	HOMO	→	LUMO	+0.65	41	2.91	426
13	HOMO-2	→	LUMO+3	+0.34	1971	3.48	357
14	HOMO-2	→	LUMO+4	+0.46	1713	3.57	347
15	HOMO	→	LUMO+4	+0.42	2903	3.58	346
15	HOMO-2	→	LUMO+3	-0.39			
40	HOMO-3	→	LUMO+3	+0.29	1436	4.46	278
68	HOMO	→	LUMO+10	+0.37	701	4.83	256
68	HOMO	→	LUMO+11	+0.26			
144‡	HOMO-25	→	LUMO+8	+0.10	158	5.44	228
170‡	HOMO-26	→	LUMO	-0.11	450	5.60	221

NC2

n	**⟨occ.orb.|**	→	**|virt.orb.⟩**	**CI coeff.**	**osc.str. ($\cdot 10^{+4}$)**	**energy/eV**	**λ/nm**
1	HOMO	→	LUMO	+0.65	42	2.51	495
11	HOMO-2	→	LUMO	+0.54	2418	3.25	382
12	HOMO-2	→	LUMO+2	+0.41	2202	3.34	372
13	HOMO-2	→	LUMO+1	+0.35	2596	3.36	369
52	HOMO-2	→	LUMO+6	+0.18	803	4.27	290
65	HOMO-1	→	LUMO+13	+0.22	1058	4.42	280
67	HOMO-1	→	LUMO+12	+0.33	936	4.46	278
75	HOMO-12	→	LUMO+1	0.26	1684	4.60	270
77	HOMO-3	→	LUMO+9	0.20	984	4.62	268
80	HOMO-9	→	LUMO+2	0.29	1546	4.65	267

† These orbital pairs are reported due to their significance for the discussion even if they are not the main contributions to transitions ***n***=144,170 of the spectrum of NC1.

Table 2 Selected optical $S_0 \rightarrow S_n$ transitions of **GIC+L** model and their orbital contributions for NC1 and NC2. The table lists the transition number (***n***), the occupied (**occ.orb.**) and virtual (**virt.orb.**) orbitals involved into the transitions, their relative contribution (**CI coeff.**), oscillator strengths (**osc. str.**), energies (**energy**), and corresponding wavelengths (λ). Calculations are performed at the cam-B3LYP/6-31++G level of theory. Full details for 45 most significant transitions of NC1 can be found in Table S1 of the ESI.

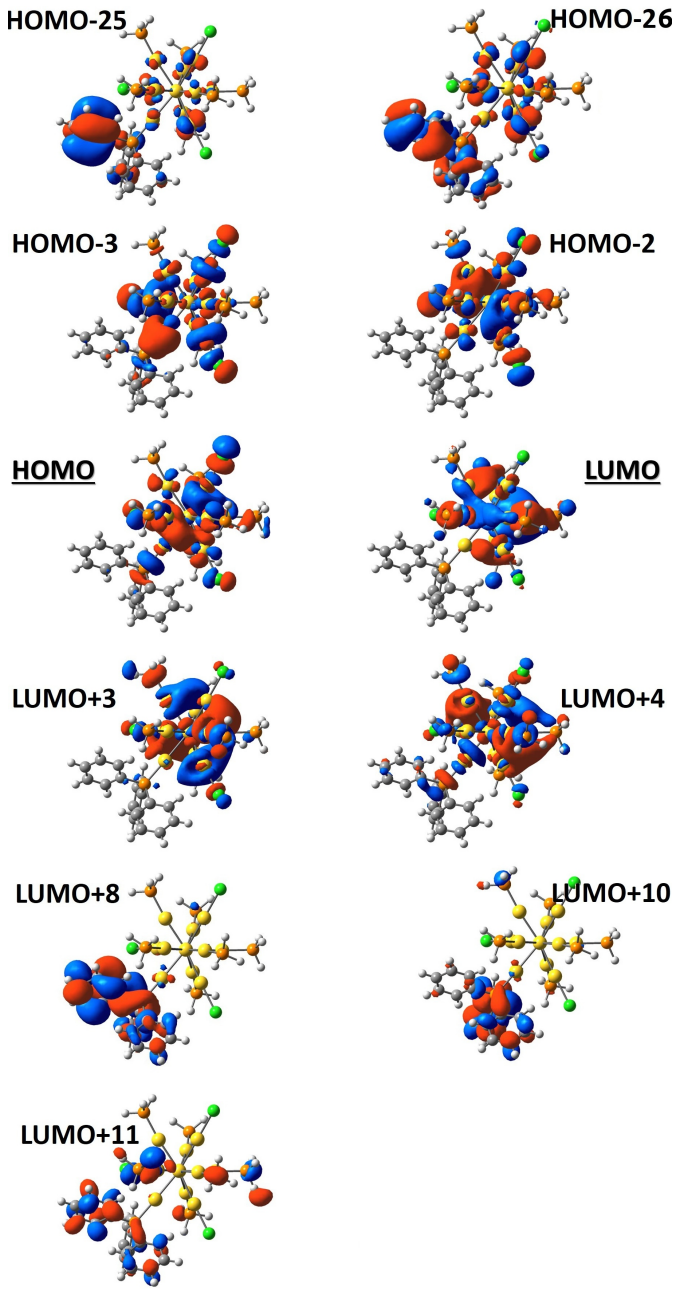

Fig. 6 Contour plots of the orbitals involved in the transitions of NC1 described in Table 2, computed at the cam-B3LYP/ 6-31++G level of theory. Blue color denotes the negative part of the DFT wavefunction, while red denotes the positive part. The underlying molecular skeleton is fixed and shown from the same point of view for better clarity, adopting the standard CPK color scheme. A more detailed description of the shape of 24 virtual and occupied orbitals can be found in Figures S5 and S6 of the ESI.

shifted of 8 nm and shows a very small oscillator strength compared to the first transition of the isolated PPh_3 molecule. Moreover, the excited state $\boldsymbol{n}$=170 presents a small contribution (CI coefficient=-0.11) given by the transition between the

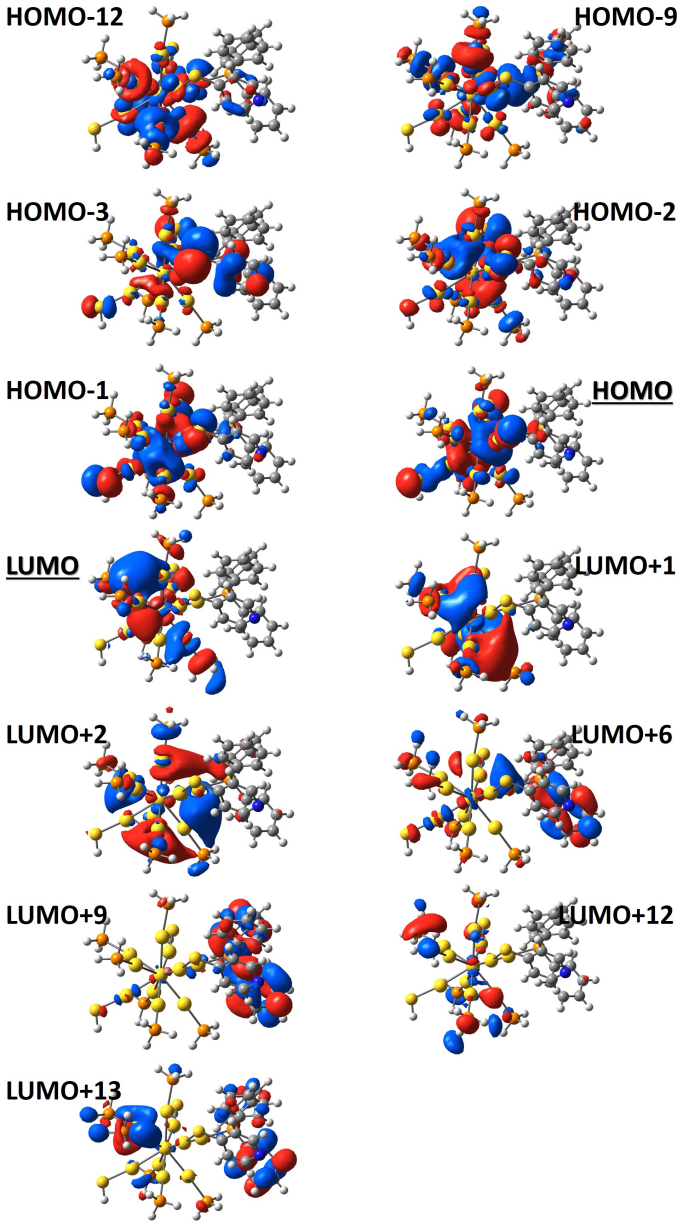

Fig. 7 Contour plots of the orbitals involved in the transitions of NC2 described in Table 2, computed at the cam-B3LYP/ 6-31++G level of theory. Blue color denotes the negative part of the DFT wavefunction, while red denotes the positive part. The underlying molecular skeleton is fixed and shown from the same point of view for better clarity, adopting the standard CPK color scheme. A more detailed description of the shape of 24 virtual and occupied orbitals can be found in Figures S5 and S6 of the ESI.

HOMO (orbital #253) and LUMO+22 (orbital #276, reported in Fig.7) that are localized on the gold core and on the PPh_3 molecule, respectively. However, it has to be highlighted that these two types of transitions occur only very sporadically in the range of energy investigated here, and that never constitute the main contribution to any absorption peak (red sticks of Fig.2). A much more detailed analysis is reported in Table S1 and Figures S5 and S6 of the ESI.

The interacting orbitals giving rise to the main optical absorption bands of NC2 (Table 2, lower panel) are reported in Fig.7. Most observations done for NC1 are still valid for NC2: in particular, most of the spectrum is due to **GIC**→**GIC** transitions, with the first **GIC**→**L** charge transfer state ($\boldsymbol{n}$=52) found at 4.27 eV. This latter energy value is about 0.53 eV lower than the corresponding **GIC**→**L** absorption peak of NC1, which is similar to the aforementioned red-shift of ∼0.56 eV observed on the HOMO-LUMO energy difference of NC2. It should also be pinpointed that some high energy transitions (≥4.6 eV) occur between states that have a non-negligible electronic density on SPyr toward the PPh_3 ligand (*e.g.* state $\boldsymbol{n}$=77).

5 Concluding Remarks

The main optical features of $Au_{11}(PPh_3)_7Cl_3$ have been correctly reproduced at increasing levels of sophistication of the model (inner core, addition of ligands, effect of the point charges) and the computational procedures adopted (functionals, basis sets for the ligands). In this way, each effect has been taken into account in order to provide a more realistic picture of the interactions occurring in the nano-cluster. The electronic properties of $Au_{11}(PPh_3)_7SPyr_3$ have been also investigated finding many similarities with the previous cluster, besides a more negatively charged metal core and a red-shift of the whole optical spectrum, which suggests that ligands induce mainly a sort of small "solvent effect" on the electronic spectra.

It appears that the optical spectra of undecagold nanoclusters are mainly due to transitions localized on metal atoms, and the atoms directly bound to them (P, Cl, and S). The optoelectronic effects due to the triphenilphosphine and thiopyridine ligands are negligible in first approximation, giving some (minor) contributions only to the higher energy band. In particular, ligand→ligand transitions are not observed in the Vis region of frequencies, and only sporadically in UV region, contrary to what has been previously reported in literature[16]. The conjugation between π-electrons of the aromatic ligands and metal electrons might occur out of the Vis region, and the experimental peak at ∼320 nm cannot be explained as due to an hypothesized red-shift of triphenilphosphine bands. In fact, the most relevant features of the spectrum can be reproduced also excluding the aromatic part of the ligand from the calculations.

The approach adopted here has been shown to be valuable to dissect optical spectra of hybrid metal-organic nano-particles, and can be extended to larger nano-systems.

6 Acknowledgements

This work was supported by the Italian "*Ministero dell'Istruzione, dell'Università e della Ricerca*" (MIUR) through the "*Futuro in Ricerca*" (FIRB) grant RBFR1248UI_002 titled "Novel Multiscale Theoretical/Computational Strategies for the Design of Photo and Thermo responsive Hybrid Organic-Inorganic Components for Nanoelectronic Circuits". The "*Programma di ricerca di rilevante interesse nazionale*" (PRIN) grant 2010C4R8M8 titled "Nanoscale functional Organization of (bio)Molecules and Hybrids for targeted Application in Sensing, Medicine and Biotechnology" is also acknowledged.

Computer time was granted through the CINECA project AUNANMR-HP10CJ027S.

References

1 R. W. Murray, *Chemical Reviews*, 2008, **108**, 2688–2720.

2 M.-S. Hu, H.-L. Chen, C.-H. Shen, H. B.-R. Hong, Lu-Sheng, K.-H. Chen and L.-C. Chen, *Nature Materials*, 2006, **5**, 102–106.

3 K. Xu, Y. Li, W. Zhang, L. Zhang and W. Xie, *Current Applied Physics*, 2014, **14**, 53 – 56.

4 M. Homberger and U. Simon, *Philosophical Transactions of the Royal Society A: Mathematical, Physical and Engineering Sciences*, 2010, **368**, 1405–1453.

5 L. Guo, Y. Xu, A. R. Ferhan, G. Chen and D.-H. Kim, *Journal of the American Chemical Society*, 2013, **135**, 12338–12345.

6 C. M. Aikens, *The Journal of Physical Chemistry Letters*, 2011, **2**, 99–104.

7 A. Tlahuice-Flores, M. Jose-Yacaman and R. L. Whetten, *Phys. Chem. Chem. Phys.*, 2013, **15**, 19557–19560.

8 M. Walter, J. Akola, O. Lopez-Acevedo, P. D. Jadzinsky, G. Calero, C. J. Ackerson, R. L. Whetten, H. Grönbeck and H. Häkkinen, *Proceedings of the National Academy of Sciences*, 2008, **105**, 9157–9162.

9 A. P. Alivisatos, *The Journal of Physical Chemistry*, 1996, **100**, 13226–13239.

10 P. Alivisatos, P. F. Barbara, A. W. Castleman, J. Chang, D. A. Dixon, M. L. Klein, G. L. McLendon, J. S. Miller, M. A. Ratner, P. J. Rossky, S. I. Stupp and M. E. Thompson, *Advanced Materials*, 1998, **10**, 1297–1336.

11 M. A. Rawashdeh-Omary, M. A. Omary and J. Fackler, *Inorganica Chimica Acta*, 2002, **334**, 376–384.

12 P. Pyykkö, *Angewandte Chemie International Edition*, 2004, **43**, 4412–4456.

13 A. Maspero, I. Kani, A. A. Mohamed, M. A. Omary, R. J. Staples and J. P. Fackler, *Inorganic Chemistry*, 2003, **42**, 5311–5319.

14 J. M. Forward, D. Bohmann, J. P. Fackler and R. J. Staples, *Inorganic Chemistry*, 1995, **34**, 6330–6336.

15 J. M. Pettibone and J. W. Hudgens, *ACS Nano*, 2011, **5**, 2989–3002.

16 Z. Wu and R. Jin, *Chemistry - A European Journal*, 2013, **19**, 12259–12263.

17 Z. Wu and R. Jin, *Nano Letters*, 2010, **10**, 2568–2573.

18 S. V. Aradhya, M. Frei, M. S. Hybertsen and L. Venkataraman, *Nature Materials*, 2012, **11**, 872–876.

19 E. Runge and E. K. U. Gross, *Phys. Rev. Lett.*, 1984, **52**, 997–1000.

20 D. Jacquemin, J. Preat, E. A. Perpète, D. P. Vercauteren, J.-M. André, I. Ciofini and C. Adamo, *International Journal of Quantum Chemistry*, 2011, **111**, 4224–4240.

21 V. V. Volkov, R. Chelli, F. Muniz-Miranda and R. Righini, *The Journal of Physical Chemistry B*, 2011, **115**, 5294–5303.

22 A. Pedone, J. Bloino and V. Barone, *The Journal of Physical Chemistry C*, 2012, **116**, 17807–17818.

23 C. Adamo and D. Jacquemin, *Chem. Soc. Rev.*, 2013, **42**, 845–856.

24 C. M. Aikens, *The Journal of Physical Chemistry C*, 2008, **112**, 19797–19800.

25 H. Häkkinen, *Nature Chemistry*, 2012, **4**, 443–455.

26 A. Nardelli, G. Fronzoni and M. Stener, *The Journal of Physical Chemistry C*, 2009, **113**, 14844–14851.

27 G. Periyasamy and F. Remacle, *Nano Letters*, 2009, **9**, 3007–3011.

28 M. R. Provorse and C. M. Aikens, *Journal of the American Chemical Society*, 2010, **132**, 1302–1310.

29 C. M. Aikens, *Molecular Simulation*, 2012, **38**, 607–614.

30 G. Piccini, R. W. A. Havenith, R. Broer and M. Stener, *The Journal of Physical Chemistry C*, 2013, **117**, 17196–17204.

31 M. Zhu, C. M. Aikens, F. J. Hollander, G. C. Schatz and R. Jin, *Journal of the American Chemical Society*, 2008, **130**, 5883–5885.

32 O. Lopez-Acevedo, H. Tsunoyama, T. Tsukuda, H. Häkkinen and C. M. Aikens, *Journal of the American Chemical Society*, 2010, **132**, 8210–8218.

33 A. Hadley and C. M. Aikens, *The Journal of Physical Chemistry C*, 2010, **114**, 18134–18138.

34 M. Muniz-Miranda, M. Pagliai, F. Muniz-Miranda and V. Schettino, *Chem. Commun.*, 2011, **47**, 3138–3140.

35 S. A. Ivanov, I. Arachchige and C. M. Aikens, *The Journal of Physical Chemistry A*, 2011, **115**, 8017–8031.

36 F. Muniz-Miranda, M. C. Menziani and A. Pedone, *The Journal of Physical Chemistry C*, 2014, **118**, 7532–7544.

37 C. L. Heinecke, T. W. Ni, S. Malola, V. Mkinen, O. A. Wong, H. Häkkinen and C. J. Ackerson, *Journal of the American Chemical Society*, 2012, **134**, 13316–13322.

38 A. Pedone, G. Prampolini, S. Monti and V. Barone, *Chemistry of Materials*, 2011, **23**, 5016–5023.

39 M. Pagliai, F. Muniz-Miranda, V. Schettino and M. Muniz-Miranda, *Progress in Colloid and Polymer Science*, 2012, **139**, 39–44.

40 G.-T. Bae and C. M. Aikens, *The Journal of Physical Chemistry C*, 2012, **116**, 10356–10367.

41 F. De Angelis, S. Fantacci, E. Mosconi, M. K. Nazeeruddin and M. Grätzel, *The Journal of Physical Chemistry C*, 2011, **115**, 8825–8831.

42 A. Pedone, G. Prampolini, S. Monti and V. Barone, *Phys. Chem. Chem. Phys.*, 2011, **13**, 16689–16697.

43 B. S. Gutrath, U. Englert, Y. Wang and U. Simon, *European Journal of Inorganic Chemistry*, 2013, **2013**, 2002–2006.

44 K. Nunokawa, S. Onaka, M. Ito, M. Horibe, T. Yonezawa, H. Nishihara, T. Ozeki, H. Chiba, S. Watase and M. Nakamoto, *Journal of Organometallic Chemistry*, 2006, **691**, 638 – 642.

45 M. J. Frisch, G. W. Trucks, H. B. Schlegel, G. E. Scuseria, M. A. Robb, J. R. Cheeseman, G. Scalmani, V. Barone, B. Mennucci, G. A. Petersson, H. Nakatsuji, M. Caricato, X. Li, H. P. Hratchian, A. F. Izmaylov, J. Bloino, G. Zheng, J. L. Sonnenberg, M. Hada, M. Ehara, K. Toyota, R. Fukuda, J. Hasegawa, M. Ishida, T. Nakajima, Y. Honda, O. Kitao, H. Nakai, T. Vreven, J. A. Montgomery, Jr., J. E. Peralta, F. Ogliaro, M. Bearpark, J. J. Heyd, E. Brothers, K. N. Kudin, V. N. Staroverov, T. Keith, R. Kobayashi, J. Normand, K. Raghavachari, A. Rendell, J. C. Burant, S. S. Iyengar, J. Tomasi, M. Cossi, N. Rega, J. M. Millam, M. Klene, J. E. Knox, J. B. Cross, V. Bakken, C. Adamo, J. Jaramillo, R. Gomperts, R. E. Stratmann, O. Yazyev, A. J. Austin, R. Cammi, C. Pomelli, J. W. Ochterski, R. L. Martin, K. Morokuma, V. G. Zakrzewski, G. A. Voth, P. Salvador, J. J. Dannenberg, S. Dapprich, A. D. Daniels, O. Farkas, J. B. Foresman, J. V. Ortiz, J. Cioslowski, and D. J. Fox, *Gaussian 09, Revision D.01*, Gaussian, Inc., Wallingford CT, 2013.

46 A. D. Becke, *Phys. Rev. A*, 1988, **38**, 3098–3100.

47 J. P. Perdew, K. Burke and M. Ernzerhof, *Phys. Rev. Lett.*, 1996, **77**, 3865–3868.

48 A. D. Becke, *The Journal of Chemical Physics*, 1993, **98**, 5648–5652.

49 C. Lee, W. Yang and R. G. Parr, *Phys. Rev. B*, 1988, **37**, 785–789.

50 Y. Zhao and D. G. Truhlar, *The Journal of Physical Chemistry A*, 2006, **110**, 13126–13130.

51 T. Yanai, D. P. Tew and N. C. Handy, *Chemical Physics Letters*, 2004, **393**, 51 – 57.

52 A. Pedone, *Journal of Chemical Theory and Computation*, 2013, **9**, 4087–4096.

53 Z.-L. Cai, M. J. Crossley, J. R. Reimers, R. Kobayashi and R. D. Amos, *The Journal of Physical Chemistry B*, 2006, **110**, 15624–15632.

54 A. Pedone and V. Barone, *Phys. Chem. Chem. Phys.*, 2010, **12**, 2722–2729.

55 E. M. M. Tan, M. Hilbers and W. J. Buma, *The Journal of Physical Chemistry Letters*, 2014, **5**, 2464–2468.

56 F. Muniz-Miranda, M. Pagliai, G. Cardini and V. Schettino, *Journal of Chemical Theory and Computation*, 2011, **7**, 1109–1118.

57 J. VandeVondele, P. Tröster, P. Tavan and G. Mathias, *The Journal of Physical Chemistry A*, 2012, **116**, 2466–2474.

58 F. Muniz-Miranda, M. Pagliai, G. Cardini and R. Righini, *The Journal of Physical Chemistry A*, 2012, **116**, 2147–2153.

59 F. Muniz-Miranda, M. Pagliai, G. Cardini and R. Righini, *The Journal of Chemical Physics*, 2012, **137**, 244501.

60 M. Couty and M. B. Hall, *Journal of Computational Chemistry*, 1996, **17**, 1359–1370.

61 K. Schuchardt, B. Didier, T. Elsethagen, L. Sun, V. Gurumoorthi, J. Chase, J. Li and T. Windus, *Journal of Chemical Information and Modeling*, 2007, **47**, 1045–1052.

62 G. Scalmani and M. J. Frisch, *The Journal of Chemical Physics*, 2010, **132**, 114110.

63 E. J. Baerends, O. V. Gritsenko and R. van Meer, *Phys. Chem. Chem. Phys.*, 2013, **15**, 16408–16425.

64 F. Hirshfeld, *Theoretica Chimica Acta*, 1977, **44**, 129–138.

65 T. Lu and F. Chen, *Journal of Computational Chemistry*, 2012, **33**, 580–592.